C. R. Physique 19 (2018) 561–574

Contents lists available at ScienceDirect

Comptes Rendus Physique

www.sciencedirect.com

Physics and arts / Physique et arts

Application of the pair distribution function analysis for the study of cultural heritage materials

Application de l'analyse par la fonction de distribution de paires à l'étude des matériaux du patrimoine culturel

Pierre Bordet

Université Grenoble Alpes, CNRS, Institut Néel, 38042 Grenoble, France

ARTICLE INFO

Article history:
Available online 31 July 2018

Keywords:
Cultural heritage materials
Pair Distribution Function
Tomography
Synchrotron

Mots-clés :
Matériaux du patrimoine
Fonction de distribution de paires
Tomographie
Synchrotron

ABSTRACT

The study of cultural heritage objects represents a challenge for materials sciences, because of their intrinsic complexity as well as because of their rare and precious nature, which requires the use of non-destructive methods. One of the major difficulties encountered by the methods of structural analysis of these materials is the presence of mixtures of crystallized and amorphous phases, the conventional methods of crystallography being poorly adapted to the latter. Here we present the Pair Distribution Function analysis method, which based on diffraction data, allows access to the identification, microstructural characterization and quantification of phases constituting a complex mixture, independently of their amorphous or crystalline character. Two recent examples will be presented to illustrate the use of this method in studies of cultural heritage materials.

RÉSUMÉ

L'étude des objets du patrimoine culturel représente un défi pour la science des matériaux, de par leur complexité intrinsèque ainsi que par leur caractère rare et précieux, qui impose d'utiliser des méthodes non destructives. Une des difficultés majeures rencontrées par les méthodes d'analyse structurale de ces matériaux est la présence de mélanges de phases cristallisées et amorphes, les méthodes classiques de la cristallographie étant mal adaptées à ces dernières. Nous présentons ici la méthode d'analyse par fonction de distribution de paires, qui, sur la base de données de diffraction, permet d'accéder à l'identification, la caractérisation microstructurale et la quantification des phases constituant un mélange complexe, indépendamment de leur caractère amorphe ou cristallisé. Deux exemples récents seront exposés pour illustrer l'utilisation de cette méthode dans le cadre d'études sur les matériaux du patrimoine culturel.

E-mail address: pierre.bordet@neel.cnrs.fr.

https://doi.org/10.1016/j.crhy.2018.06.001

1. Introduction

In the transdisciplinary investigation of cultural heritage and archaeological artefacts, physical-chemical science methods provide means to access all material aspects related to chemical/structural composition, microstructure, spatial distribution of phases, etc. Interpreting this information can help revealing the source of constituting materials, the way they were used and transformed and their evolution over time. However, working on such types of objects entails quite unusual constraints for the materials scientist, mainly due to the rare and precious nature of the samples. It is necessary to apply a large range of characterization techniques to a single, often minute, sample that must be left intact. In this respect, X-ray-based techniques have proven to be extremely efficient, either for chemical analysis using fluorescence detection or for phase identification and quantization using diffraction and crystallography. These methods, as well as the study of cultural heritage materials, have greatly benefitted from the appearance of third-generation synchrotron sources, allowing more precise and faster measurements of always smaller samples. Also, they have led to the development of new techniques, such as 3D tomographic imaging using either absorption, fluorescence, or diffraction signals. Here we will focus on a technique related to X-ray diffraction: the Pair Distribution Function (PDF) analysis, based on the measurement of total scattering data, a method that was originally used in the laboratory for the study of amorphous compounds, but which is now quickly extending to many fields of materials research thanks to methodological and software developments and the access to high energy X-ray sources, particularly synchrotrons. The special merit of this method is to give access to quantitative information on the structure, coherence length and phase content in complex mixtures independently of the amorphous or crystalline nature of the compounds. This opens the way to analysis of amorphous or nanocrystalline phases in cultural heritage objects, such as varnish, resins, organic binders, nanocrystalline minerals, etc., which were previously overlooked in classical crystallographic studies based on Bragg scattering.

In the following, I will first briefly present the PDF analysis method, giving also a quick introduction on Diffraction/Scattering Computed Tomography (DSCT), which may be a very important complementary tool for the case of multiphase compounds. I will then present two examples of application of PDF analysis in the context of cultural heritage material taken from the literature: the fading of ancient Prussian blue pigments and the investigation of archaeological carbon blacks from the Roman period.

2. Total scattering and the pair distribution function

Historically, as described in the books by Guinier [1] or Warren [2], the pair distribution function was used to characterize the local order in amorphous compounds using data from wide-angle X-ray scattering. Indeed, this function is somehow a histogram of interatomic distances in a compound, regardless of its crystalline or amorphous state. Experimentally, it is obtained by the sine Fourier transform of a powder diffraction pattern. For a long time, the main limitation was the possibility of obtaining diffraction data up to large $Q = 4\pi \sin\vartheta/\lambda$ to limit the cut-off effects of the Fourier transform. This requires working with short wavelengths less accessible to laboratory instruments and has long restrained the use of the PDF to the field of amorphous materials and liquids. More recently, PDF analysis took a new development thanks to its usefulness in the study of local structure and nano-materials, to the availability of high-energy sources and instruments at synchrotrons and neutron facilities, even in the laboratory, and to the development of user-friendly software to process and analyze the data.

Depending on the authors and communities, there are different definitions of the pair distribution function. See for example [3], where relationships between different definitions are explained. We will follow herein the formalism developed by Egami and Billinge [4]. The PDF $G(r)$ yields the probability of finding a pair of atoms separated by a distance r in a sample. It can be calculated from a structural model describing the distribution of atoms in the sample according to the formula:

$$G(r) = \frac{1}{r}\sum_i \sum_j \left[\frac{b_i b_j}{\langle b\rangle^2}\delta(r - r_{ij})\right] - 4\pi r\rho_0 \tag{1}$$

where the sum is propagated over the atoms contained in the structural model, separated by a distance r_{ij}. b_i is the scattering power of atom i (i.e. its form factor for X-rays); $\langle b\rangle$ is the average scattering power of the sample; ρ_0 is the numerical density, i.e. the number of atoms per unit volume. This function will present peaks for values of r corresponding to the interatomic distance in the model, the intensity of these peaks being proportional to the product of the scattering factors of the atoms forming the pair. All the contributions of all pairs of atoms add up in the PDF. The position of the peaks reflects the distribution of interatomic distances in the material. From Eq. (1), the contribution of each pair consists in a δ-function. The second term, $-4\pi r\rho_0$ in Eq. (1), is a normalization term introduced to compensate for the increase of the average number of atomic pairs with r, given the numerical density ρ_0. For a completely random distribution of atoms, the PDF will then be flat and equal to 0 for any r. In a real case, the frequent (i.e. more than average) presence or absence of interatomic distances appears as fluctuations of the PDF about zero. For short distances corresponding to close atomic neighbors, isolated peaks can be observed. They can be interpreted using a Gaussian statistical distribution of distances in the sample around a single average value. The width of the peaks directly reflects the width of the distribution, which may be due to thermal vibrations or some disorder induced dispersion.

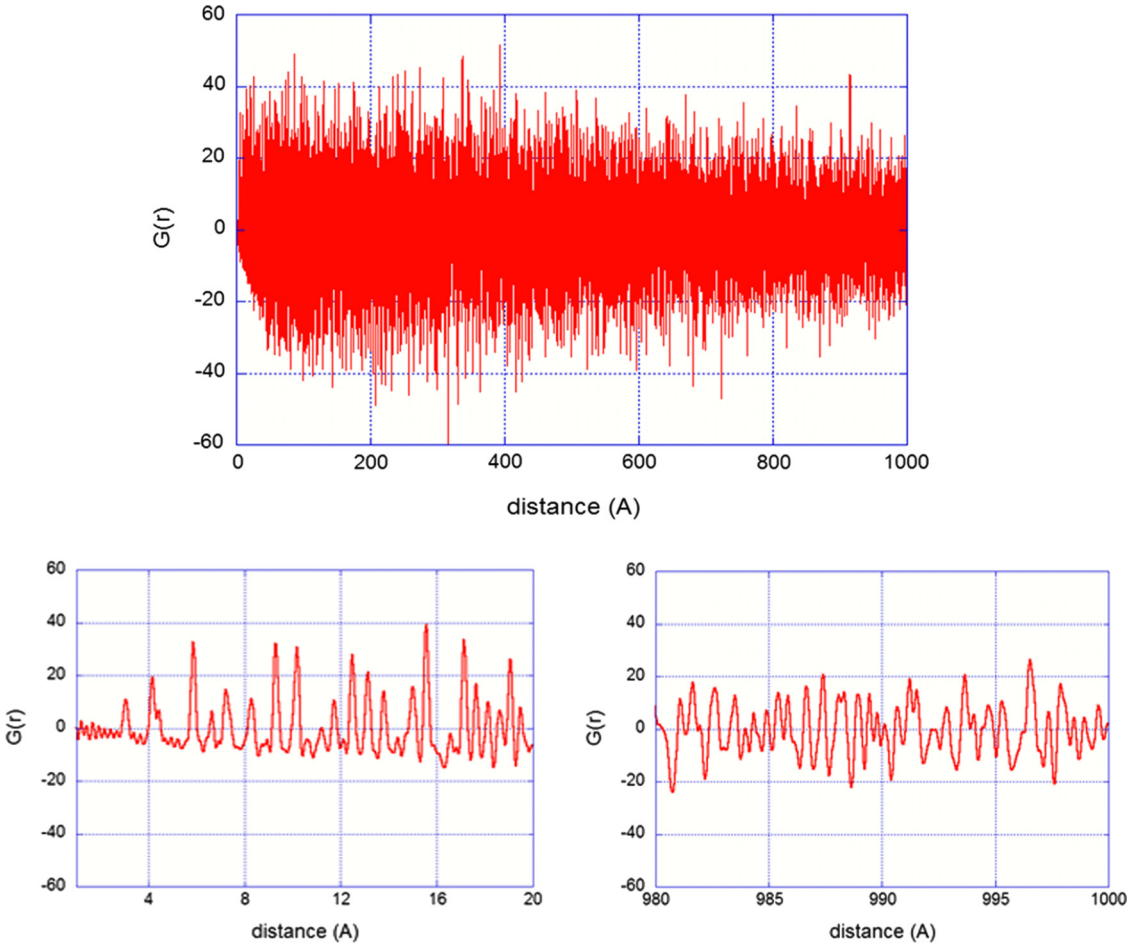

Fig. 1. Experimental PDF for LaB6 obtained up to 1000 Å from data collected at the ESRF ID31 beam line, $E = 35$ keV. Below are shown details of the PDF between 1–20 Å (left) and 980–1000 Å (right).

For a crystalline solid, the distribution of interatomic distance is defined by the coordinates of atoms, the atomic displacement parameters, and the periodicity of the unit cell. The PDF will yield a peak at each of these distances, the width of the peak being related to the atomic displacement parameters of the atoms forming the pair, and its surface to the product of their scattering powers.

In principle, the PDF will show peaks or oscillations up to the largest interatomic distances forming a coherent structure in the sample. For a well-ordered material, this can extend up to very long distances (Fig. 1).

In the case of nanoparticles, the sets of coherently scattering atoms are limited to the volume of the individual particles, and therefore no peak in the PDF will be observed above the longest interatomic distance within the particles. Above this distance, only randomly distributed interatomic distances between atoms belonging to different particles will exist, and the PDF will vanish due to the normalization term of Eq. (1). The PDF will thus provide a direct estimate of the particle size, plus the distribution of interatomic distances inside the particles. The result will be similar for amorphous compounds: the PDF will vanish with the loss of structural coherence induced by disorder. The case of titanium oxide nano-particles of a diameter less than 1 nm is exemplified in Fig. 2 for PDF data obtained using a laboratory diffractometer in Bragg–Brentano geometry and Mo Kα radiation. A particle size of ~8–9 Å can be readily deduced by simple observation of the PDF; a model of atomic arrangement inside the particle can be checked and fitted to the data to identify the phase and provide a quantitative determination of interatomic distances.

Experimentally, the PDF is obtained from a powder diffraction pattern by realizing the Fourier transform as:

$$G(r) = 4\pi r\big[\rho(r) - \rho_0\big] = \frac{2}{\pi}\int_0^\infty Q\big[S(Q) - 1\big]\sin(Qr)\,\mathrm{d}Q \tag{2}$$

where $\rho(r)$ is the microscopic pair density, $S(Q)$ is the total structure function, i.e. the normalized coherent scattered intensity. It is worth noting that the whole diffraction pattern is used to obtain $G(r)$, not only the Bragg peak intensities as for

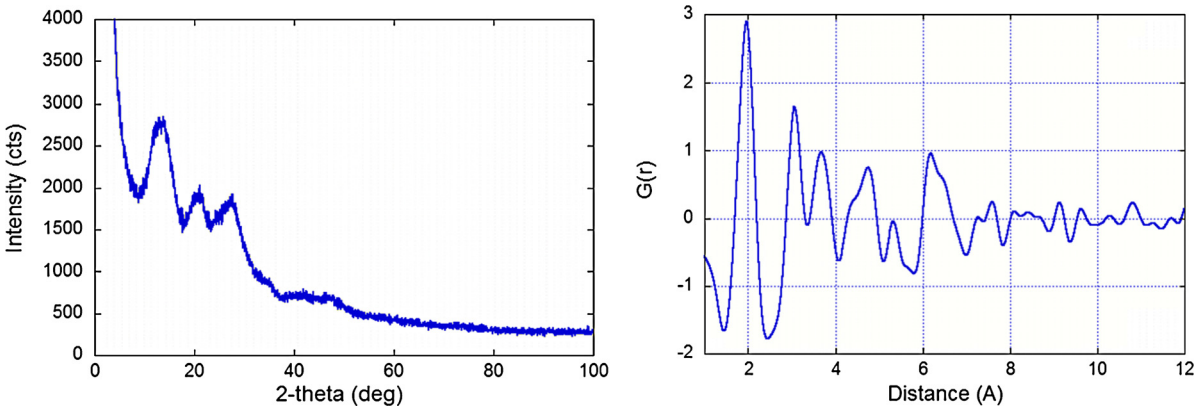

Fig. 2. Left: part of the diffraction pattern for nano-crystalline titanium oxide measured up to $2\vartheta = 150°$ on a laboratory diffractometer with Bragg–Brentano geometry and Mo Kα radiation. Right: the corresponding PDF.

a classical crystallographic analysis. This is why such type of data is often referred to as "total scattering" data. Therefore, the effects of disorder, defects, etc., which contribute to the pattern through diffuse scattering outside of the Bragg peaks, will also be included in $G(r)$. Obtaining $S(Q)$ from diffraction data requires to perform a set of corrections to eliminate all incoherent (Compton) or inelastic (fluorescence...) contributions, the signal coming from the environment (sample holder, cryostat, air scattering, etc.), as well as the effects of the absorption, multiple scattering, etc. These corrections require additional measurements of these contributions (empty sample holder, etc.). The self-scattering contribution is then subtracted and the pattern is normalized by $\langle b\rangle^2$, resulting in $S(Q)$. Then the function $F(Q) = Q \cdot (S(Q) - 1)$ is Fourier transformed according to Eq. (2). User-friendly programs to calculate the PDF from experimental patterns are now available for neutrons as well as X-rays, and the procedure has become almost routine.

In order to minimize detrimental effects brought about by the Fourier transform (termination ripples, peak broadening, normalization errors, etc.) that can lead to misinterpretations of the data, it is necessary to collect diffraction patterns up to sufficiently high maximum Q values, Q_{max}. Moreover, due to the decrease vs Q of the scattering power in the case of X-rays, the normalization of $S(Q)$ by dividing with $\langle b\rangle^2$ will significantly amplify the data at large Q. It is therefore important to ensure sufficiently high counting statistics at high Q values, otherwise a high noise level at high Q for $F(Q) = Q(S(Q) - 1)$ will introduce a strong spurious signal in the Fourier transform and therefore the PDF. To obtain a powder diffraction pattern usable for PDF analysis, one must combine a high Q_{max} (meaning small-wavelength/high-energy radiation) and high counting statistics on a wide Q range. Both conditions can be fulfilled at synchrotron sources. One solution is to use a parallel-beam high-resolution powder diffraction setup (e.g., ID22 at ESRF, CRISTAL at SOLEIL, etc.) with the advantages of eliminating the inelastic/incoherent scattering and to obtain PDFs that can extend over very long-distance ranges of several hundreds of Å (Fig. 1), but leads to yet long measurement times (several hours). The alternate set up relies on the access to very high energies (~100 keV) at which a flat plate 2D detector allows one to collect data to high Q in a short time (for example at ESRF beam lines ID11, ID15, ID22, ID31, etc.). In this case, although the spatial resolution is poorer and the PDFs hardly extend over 100 Å, in situ studies, investigations of phase transitions, solidification, etc. become feasible. An intermediate solution for moderately high-energy beamlines in the 20–30 keV range is to take diffraction images with a 2D detector at increasing values of 2ϑ, which are then integrated and combined to get a diffraction pattern used to compute the PDF. In such a case, the collection time may be less than one hour and the spatial resolution is controlled by the adjustable sample to detector distance. This method is used for example at the BM02-ESRF and CRISTAL-SOLEIL beamlines.

As seen above, the PDF can be obtained experimentally from total scattering measurements and can also be calculated provided some kind of distribution of atoms is given. In principle, it is therefore possible to identify a compound from its PDF, which may represent a kind of fingerprint, as was shown for the case of pharmaceutical materials [5,6]. It can also be used to determine the structural coherence length or the nanoparticle size. In the case of mixtures, since the total PDF is the sum of the PDFs of the different phases weighted by their proportions in the mixture, it can be used for quantitative analysis, independently of the crystalline and/or amorphous nature of the phases.

To extract quantitative information from the PDF, the technique better adapted to the case of cultural heritage materials (e.g., program PDFGui [7]) consists in a least squares profile refinement of the experimental PDF with a periodic structural model, sort of Rietveld refinement in direct space (Fig. 3), using software such as PGFGui [7] or MolPDF [8]. Symmetry constraints can be imposed and refinements can be applied to different ranges of distances, to compare local and average structure. The effects of various instrumental (Q_{max}, spatial resolution...) and sample-dependent parameters (atomic displacement correlations, structural coherence length...) can be applied. The model can also comprise several different phases with individual scale factors, allowing quantitative analysis to be performed regardless of the crystalline state of the different phases. With MolPDF, restraints on interatomic bonds and angles can be applied, allowing the refinement of complex molecular structures.

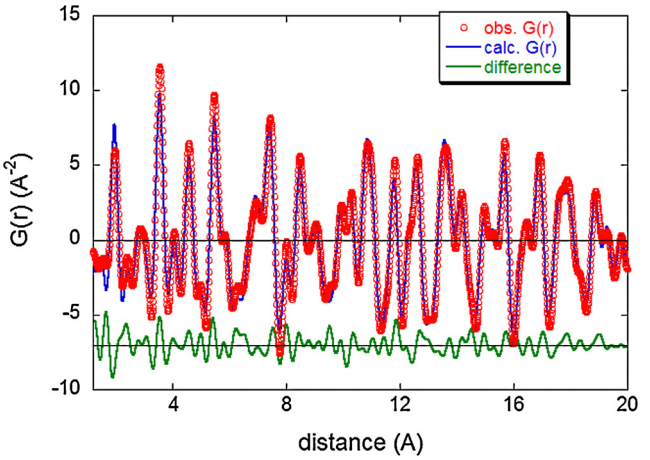

Fig. 3. Refinement using PDFGui software of the PDF of rutile from data measured up to $2\vartheta = 150°$ on a laboratory diffractometer with Bragg–Brentano geometry and Mo Kα radiation.

Thus, for archeological or cultural heritage samples containing non-crystalline phases, this technique can be extremely useful, since it provides means for identifying, quantifying and characterize the microstructure of amorphous as well as crystalline phases in a complex sample.

3. Diffraction/scattering computed tomography

In the case of very complex mixtures often encountered in archaeological samples, Diffraction/Scattering Computed Tomography (DSCT) is a valuable tool to separate the contribution of each individual phase and reconstruct its powder diffraction pattern. As it is well known, absorption tomography gives insights into the three-dimensional density repartition within the material, and similar reconstructions can be made using the fluorescence signal, which yield the 3D map of chemical elements in a sample [9]. On the other hand, the DSCT technique, by using diffraction images for the tomographic reconstruction, is sensitive to the crystalline state and structure. It has been now implemented on several synchrotron beamlines and even on laboratory instruments ([10,27] and references therein). For such data collection, the sample, mounted for instance inside a capillary, is scanned with regular steps along a translation direction transverse to the beam. For each translational step, 2D diffraction images are recorded at successive axial rotation angles. The rotation and translation steps are chosen according to the desired resolution of the reconstruction (3D size of the voxels in the reconstructed image), and also depend on the beam size. The images are then integrated to give 1D powder patterns that are processed to yield the 3D reconstruction of the object, showing the spatial distribution of the different phases in the sample. Images showing the location of a particular phase can be produced by selecting a feature in the diffraction pattern (Bragg peak, amorphous hump ...) to which only this phase contributes. By combining the diffraction patterns corresponding to the voxels where only this phase is present (reverse analysis), one can reconstruct its single-phase powder pattern. In principle, this is possible even for minor constituents of a mixture, thereby greatly facilitating their identification and even allowing Rietveld structure refinement. Fig. 4 shows the experimental setup for a typical multimodal tomographic experiment including absorption, fluorescence and diffraction signals recorded simultaneously during tomographic displacements.

If the DSCT data are collected to sufficiently high Q_{max}, it is also possible to carry out PDF analysis from powder patterns that have been reconstructed in this way [11].

4. Examples

Until now, the use of PDF analysis in the context of cultural heritage materials remains quite seldom. I present below two examples taken from the literature and to which I collaborated, where the role of PDF analysis and DSCT are emphasized to demonstrate the interest of using these emerging techniques in this field.

4.1. Structure of Prussian blue and fading of ancient Prussian blue pigments investigated by PDF analysis

Prussian blue (PB) pigments are mixed-valence iron(III) hexacyanoferrate(II) complexes of typical stoichiometry $Fe_4^{3+}[Fe^{2+}(CN)_6^-]_3 \cdot xH_2O$ or $KFe^{3+}[Fe^{2+}(CN)_6^-] \cdot xH_2O$ that have been used as pigments in oil paintings and watercolors for 300 years since their accidental discovery in Berlin in 1704. Even though all PBs are highly insoluble, the alkali-free PB is commonly referred to as the insoluble Prussian blue, whereas Prussian blues containing alkali cations are called soluble PB's. PB's and their analogues containing other transition metal cations have been recently subject to intense research activities to elucidate the physical behavior related to their mixed valence nature, as for example the intense blue color of PB is

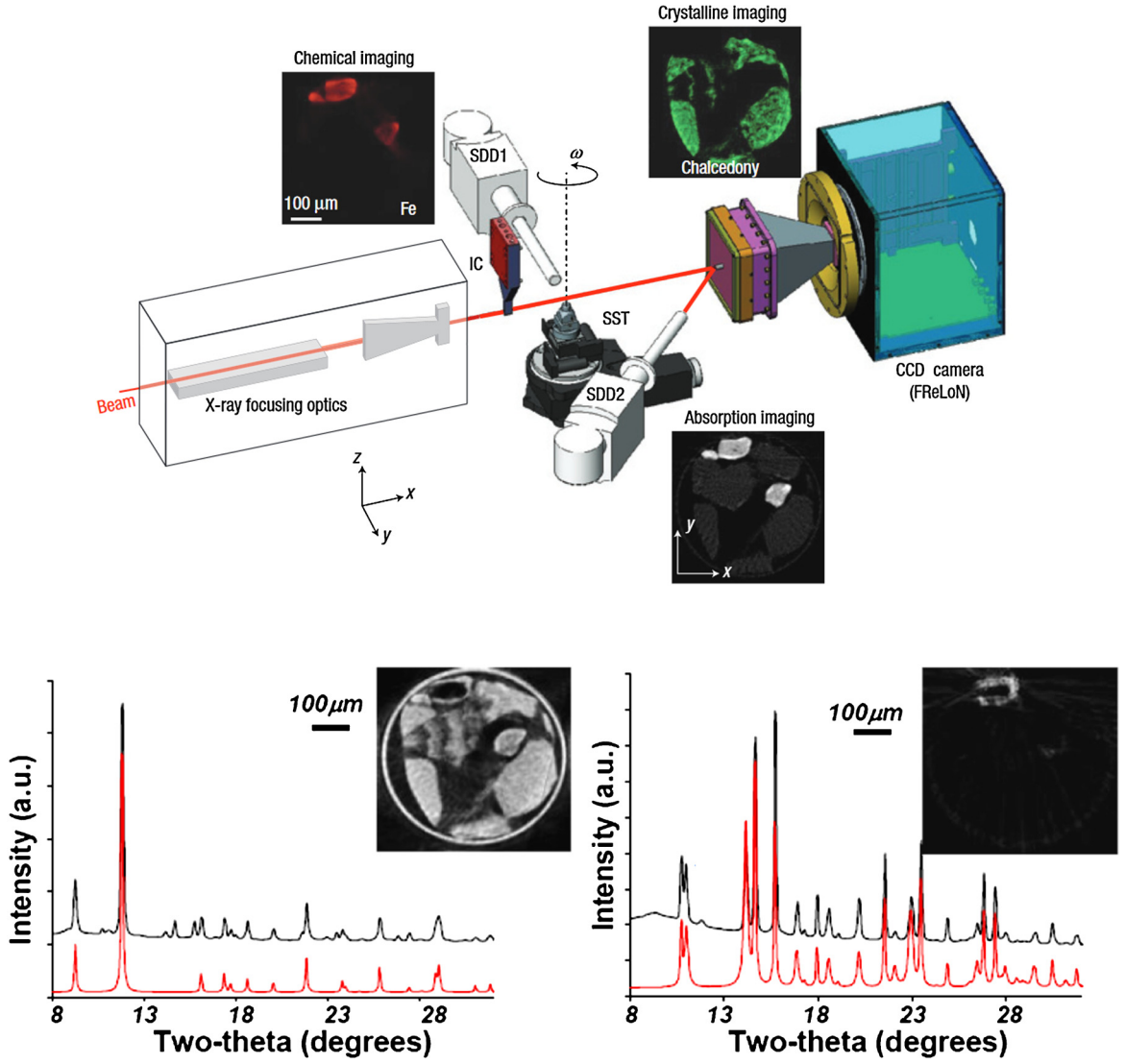

Fig. 4. Top: experimental setup for DSCT ("diffraction-tomography"). An X-ray beam is focused on the sample positioned on a support allowing rotation and translation movements. Several quantities are measured simultaneously: the fluorescence signal (SSD1), transmitted intensity (SSD2) and scattered radiation (CCD camera). Bottom: two images of the same powder containing chalcedony and various iron pigments obtained by selecting one or more of its components, as well as experimental (black) and calculated (red) diffracted intensities. Left: complete image; right: the highlighting of a grain formed of hematite and siderite (adapted from [10]).

due to an electron transfer from Fe^{2+} to Fe^{3+} cations in different crystallographic environments when light is absorbed at ca. 700 nm. Nevertheless, our knowledge of the PB crystal structure remains incomplete, due to the presence of vacancies and disorder. Although PB pigments were very rapidly of wide use in paintings, because of their intense color and low cost, problems of discoloration and fading were soon reported. They were attributed to a poor control of the preparations based on cooking-like recipes, which for example involved animal blood as source of iron. This problem was eliminated in the 1850s thanks to new synthetic methods based on rational chemistry knowledge. However, the precise origin of fading in ancient PB's is still not clearly understood. This is an important issue for restauration and conservation of many 18th–19th-century paintings.

Recently [12], a thorough investigation aiming to elucidate the origin of fading of ancient PB pigments was conducted, based on the comparison of modern, commercial materials with samples obtained in the laboratory following ancient recipes. All samples were submitted to a wide range of physical-chemical characterizations involving fading measurements, Extended X-ray Absorption Fine Structure, Particle-Induced X-ray Emission, Raman, UV-visible light spectroscopies and X-ray Powder Diffraction. Since these compounds were found to exhibit local vacancy ordering and some of the samples produced with ancient recipes yielded amorphous-like XRPD patterns, PDF analysis of synchrotron total scattering data was used to investigate their structures.

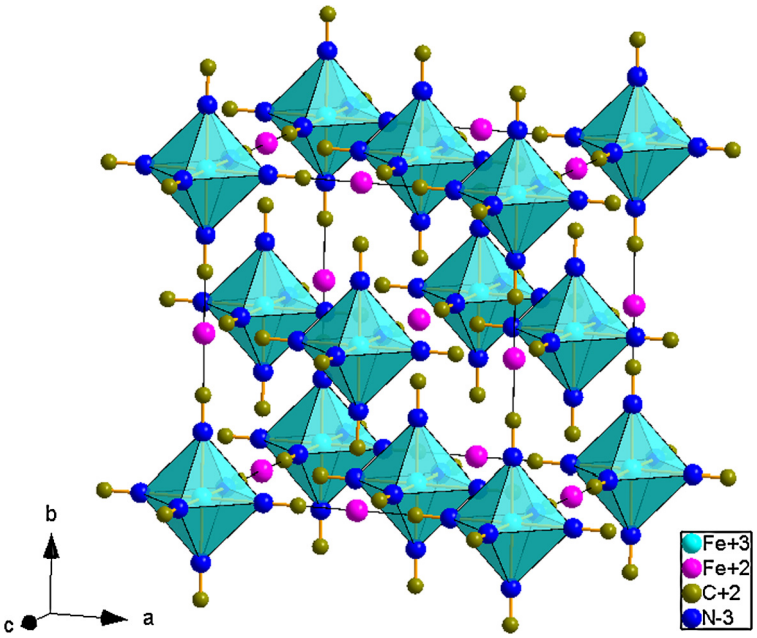

Fig. 5. The crystal structure of insoluble Prussian blue. Water molecules have been removed for clarity.

4.1.1. The local structure of modern Prussian blue pigments

PB was originally described in a cubic $Fm\bar{3}m$ symmetry (Fig. 5), with 4 Fe^{3+} cations placed on the 4a position at the origin of the unit cell and 3 $[Fe^{2+}(CN)_6^-]$ located on the 4b (1/2 1/2 1/2) position with an occupancy of 3/4 [13]. In the "insoluble" PB, two types of water molecules are observed: zeolitic water at the 8c (1/4 1/4 1/4) position and structure water substituting for the cyanoferrate complex at the 24e position ($x \sim 0.25$ 0 0). In the "soluble" PB, the potassium cations are partly substituting the zeolitic water molecules. However, single-crystal diffraction studies have shown that additional reflections breaking the F centering can be observed, which may be attributed to partial ordering of the vacancies on the 4b position [14]. The structure was then described with the $Pm\bar{3}m$ space group, for which the 4b position in $Fm\bar{3}m$ splits into the 1b (1/2 1/2 1/2) position with occupancy p and the 3d (1/2 0 0) position with occupancy $(1 - p/3)$. This distribution maintains the 3/4 global occupancy of the hexacyanoferrate complexes necessary for charge balance, while allowing for differences of occupancies for the two sites, justified by refinements with the $Pm\bar{3}m$ symmetry. For $p = 3/4$, the occupancies of both 1b and 3d positions are equal, corresponding to full vacancy disorder, and the $Fm\bar{3}m$ symmetry is observed.

Using Synchrotron Powder Diffraction Data collected at the CRISTAL-SOLEIL beamline on samples of soluble and insoluble PB commercial pigments, Samain et al. [15] did not observe the F-center breaking reflections. However, their Rietveld refinements were markedly superior using $Pm\bar{3}m$ symmetry, leading to $p = 0.72$ for the soluble (i.e. K-containing) pigment, and $p = 0.61$ for the insoluble one. This indicates that, at least for the insoluble PB, vacancy ordering occurs in the material since p is significantly different from the 3/4 value corresponding to a random distribution. However, the absence of reflections breaking the F-centering indicates that this vacancy ordering should be only very short range. PDF analysis is then the tool of choice to confirm the existence of local vacancy ordering in these compounds. This was carried out on the same samples previously studied at SOLEIL using total scattering data collected at the ID11-ESRF beamline using a 2-D detector and 100-keV photons. Fig. 6 shows the PDFs obtained using PDFGetX2 [17] for both commercial soluble and insoluble PB. The close resemblance of both curves indicates very similar structural arrangements for both compounds. The fast decay of the PDF is due to instrumental resolution.

Refinements of the PDF in a "direct space Rietveld" fashion were carried out with the PDFGui software [7] starting from the average structures obtained previously. Fig. 7 shows the result of the refinement for the soluble PB sample using constrained partial occupancies with a p value fixed at 0.72 for distances between 10 and 25 Å. The agreement is excellent, showing that the average description is consistent with the PDF data for distances above the cell parameter.

On the other hand, Fig. 8 shows the agreements obtained by applying the structures previously refined in the 10–25 Å range to the 1–10.5 Å range covering one unit cell, for both samples. Obviously, the agreement is much poorer. A usual way to interpret such discrepancies is to invoke local structural distortions, which are averaged in the average structure and thus no longer detectable in the PDF at sufficiently long distances, as well as in Rietveld refinements. The PDF calculated at short distances is then an experimental check for the existence of such distortions, and a powerful tool to understand and quantitatively characterize them. However, in the case of PB pigments, the interpretation is complicated by the presence of vacancies. Whereas in the average structure crystallographic description, atomic sites can be affected by a partial occupancy parameter to consider the presence of vacancies or substitution, at the local scale of a unit cell, occupancy can be only 0

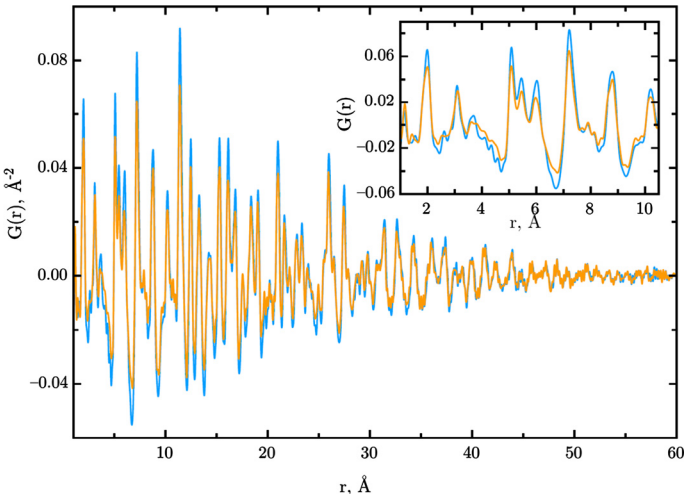

Fig. 6. PDF of insoluble (blue) and soluble (orange) Prussian blue pigment obtained at the ID11-ESRF beamline. The short-distance range is shown in the inset.

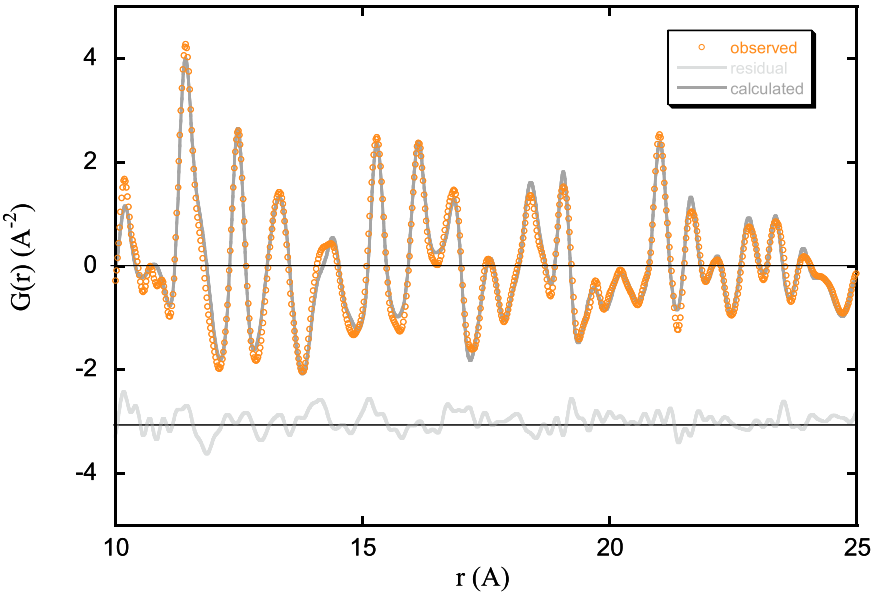

Fig. 7. PDF refinement of the soluble Prussian blue pigment from ID11-ESRF data for distances in the range from 10 to 25 Å using the average structure model.

or 1, i.e. an atom is present or not. Thus, the calculation of the PDF at very short range should not imply partial occupancies, otherwise aberrant distances may appear. For example, in the case of PB pigments, distances between the Fe^{2+} cations of the hexacyanoferrate complexes and oxygen atoms from the neighboring water molecules that substitute for them will be present at ∼2.95 Å in the PDF calculated with the average structure, although they cannot exist in the local structure and are then absent from the observed PDF. A way to circumvent this problem is to refine the local PDF by using several phases in which all atom sites have full occupancy, but with different compositions and scale factors reflecting the average stoichiometry.

In the case of PB, Herren et al. [18] showed that the average structure can be described as the superposition of five types of unit cells containing 0, 1, 2, 3 or 4 vacancies on the 4b positions of the $Fm\bar{3}m$ space group and calculated the probability of occurrence of each type of cell for a random distribution with 3/4 average occupancy, leading to values of 0.316, 0.422, 0.211, 0.047, 0.004, respectively. The PDF data were then refined using the three more probable types of unit cells, containing 0, 1 or 2 vacancies, which lead to a substantial improvement of the agreement between observed and calculated PDFs, as shown in Fig. 9. Although the refinements were carried out formally in $P1$, the atomic positions and cell parameters were still constrained to the cubic $Pm\bar{3}m$ symmetry to limit the number of parameters. However, it is clear that such symmetry cannot be respected locally for unit cells containing 1, 2, or 3 vacancies, so that the result obtained

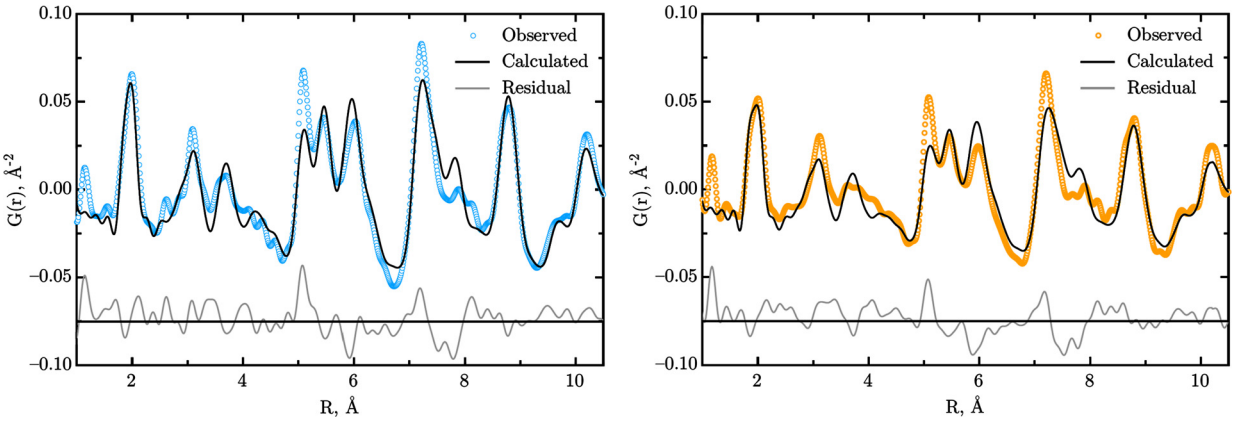

Fig. 8. PDF refinements of the soluble (blue) and insoluble (orange) Prussian blue pigments from ID11-ESRF data for distances in the range from 1 to 11 Å using the average structure model.

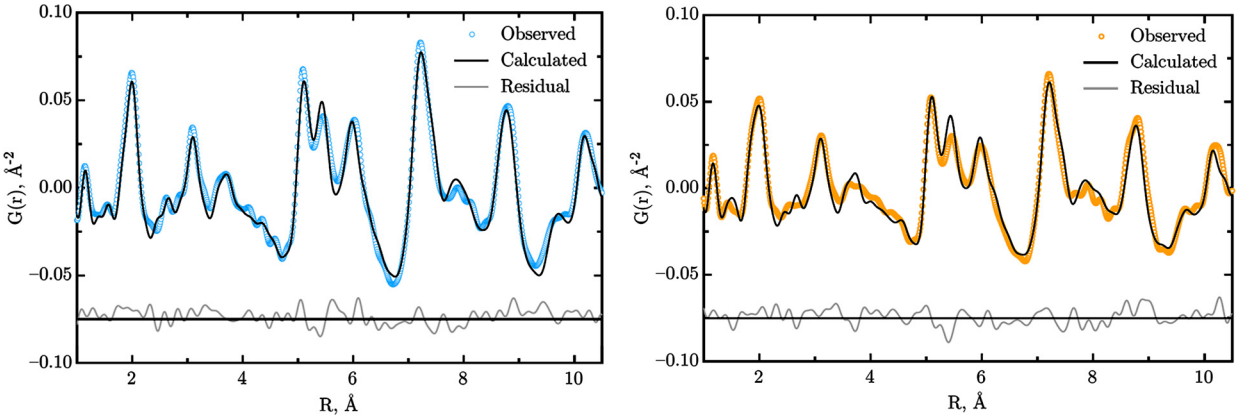

Fig. 9. PDF refinements of the soluble (blue) and insoluble (orange) Prussian blue pigments from ID11-ESRF data for distances in the range from 1 to 11 Å using a three-phase model with unit cells containing 0, 1, or 2 hexacyanoferrate(II) complex vacancies.

here is only approximate, and more work is required on better crystallized samples to progress in the understanding of the local structure of PB pigments. Nevertheless, for the samples investigated here, most of the features of the PDFs at short distances can be accurately described using this simplified model. It is interesting to note that, for both samples, the probabilities for each type of unit cell refined to about 15, 35 and 50%, indicating a strong decrease of probability for unit cells with no vacancies and a corresponding increase of the probability of unit cells with two vacancies with respect with the random distribution. This tendency to favor unit cells with an intermediate number of vacancies, implying a non-random distribution, may be at the origin of the symmetry lowering from $Fm\bar{3}m$ *to* $Pm\bar{3}m$. This effect would be better observed in well-crystallized samples, in which similar local distortions induced by vacancy ordering could extend over larger domains.

4.1.2. PDF investigation of Prussian blue analogs

During the same experiment [15,16], PDF data were also collected for samples of soluble Prussian Blue prepared by using methods equivalent to those reported in 18th-century recipes from Dossie [19] and Le Pileur d'Apligny [20]. The methods involved heating a mixture of dried blood and alkali, followed by addition of iron salt and alum and acid treatment. Fig. 10 shows the diffraction patterns from a selection of samples, compared with the same commercial soluble PB sample reported above. Their synthesis methods, labels, and appearance are described in Table 1. In some cases, an acidic treatment was used to remove Al-containing phases, sought to be mainly Al hydroxide.

Obviously, the best results in terms of the typical PB intense dark blue color was obtained for the samples yielding a diffraction pattern similar to that of commercial PB, the color being more intense when the crystalline quality is improved. Especially those samples to which alum was added ($KAl(SO_4)_2 \cdot 12H_2O$) yielded only light blue, greenish or even brown color, and their diffraction pattern did not contain any Bragg peak. The LPA2 sample, although not containing alum, shows the presence of the PB diffraction peaks over a large diffuse background.

The corresponding PDFs measured at the ID11-ESRF beamline are shown on the right-hand side of Fig. 10. Using PDF analysis, we hoped to verify whether the non-crystalline samples did conserve a PB-like structure at the local scale and/or identify possible amorphous phases or mixtures. As expected, the LPA1 and D1 samples exhibit a PDF very similar to that

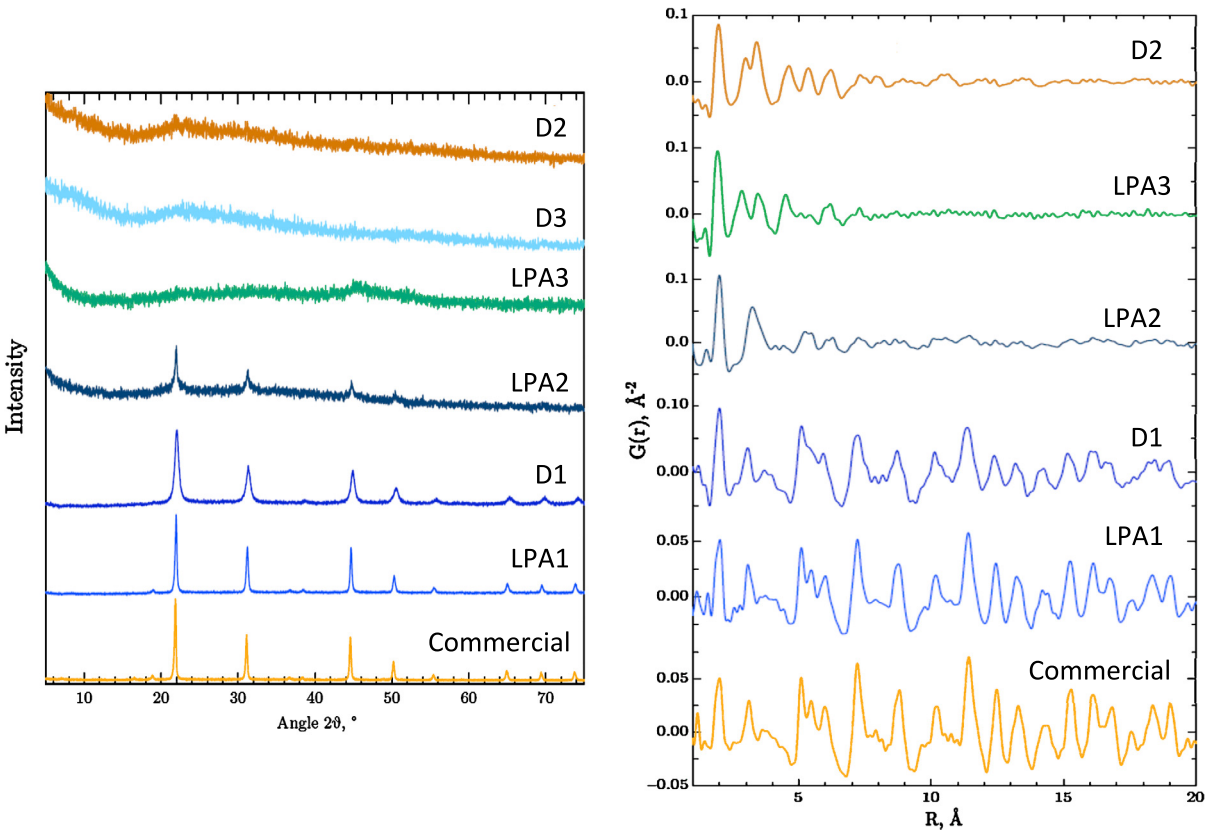

Fig. 10. Left: X-ray diffraction patterns (Fe Kα radiation) and right: X-ray PDFs (ID11-ESRF) from Prussian blue samples obtained from 18th-century recipes. The data for a commercial soluble PB sample are added for comparison.

Table 1
Description and labels of the laboratory-synthesized Prussian blues using 18th-century recipes.

Ancient author	Synthesis	Label	Color appreciation
Dossie	Immediate filtration, acid treatment	D1	Dark blue
Dossie	No acid treatment, Al containing phase	D2	Light blue-green
Dossie	No acid treatment, Al containing phase	D3	Light blue
Le Pileur d'Apligny	Immediate filtration, acid treatment	LPA1	Intense dark blue
Le Pileur d'Apligny	Delayed filtration, acid treatment	LPA2	Dark blue-gray
Le Pileur d'Apligny	No acid treatment, Al containing phase	LPA3	Brown

of commercial PB, D1 being affected by a higher level of disorder, as indicated by the broadening of the PDF peaks, and a shorter structural coherence length, as indicated by a faster decay of the PDF at large distances. For the other three samples, their PDFs show very small coherence lengths between 1 and 2 nm and, even at the very local scale, the PDFs hardly resemble that of PB, indicating that very probably at least another amorphous compound in present. This could particularly be the case of the LPA2 samples, for which the PB Bragg peaks are clearly visible on the diffraction pattern, although the short-distance PDF is markedly different from the PB one. ^{57}Fe Mössbauer spectroscopy on the same samples showed in the top four ones in Fig. 10 (right) the presence of a quadrupole doublet which was attributed to ferrihydrite [16]. Ferrihydrite is an orange color, poorly-ordered hydrous iron(III) oxide of chemical formula $Fe_5HO_8{\cdot}4H_2O$ [21], with hexagonal symmetry (space group: $P6_3cm$, $a = 5.95$ Å, $c = 9.06$ Å) [22].

However, Mössbauer spectroscopy can hardly univocally identify such a phase, and it is only sensitive to iron-containing compounds. To ascertain the presence of ferrihydrite, the LPA2 sample showing both a relatively well-crystallized PB phase and an unidentified amorphous phase was studied by DSCT at the BM02 French CRG beamline of the ESRF, using a 100 × 100-μm^2 beam and a CCD detector to record diffraction images at $E = 17.7$ keV ($\lambda = 0.7$ Å). A solid fragment of the sample was blocked inside a 1-mm quartz capillary. After 3D reconstruction of the tomography and localization of the different phases in the sample, only the voxels where a single phase was present were used to generate powder diffraction patterns of the individual phases present in the sample. Essentially two main phases could be identified: a relatively well-crystallized Prussian blue phase, and a nanocrystalline compound that could be clearly identified as ferrihydrite from the position of the Bragg peaks. For the Al-containing samples, the similarity of the PDF with that of ferrihydrite led us to suppose that

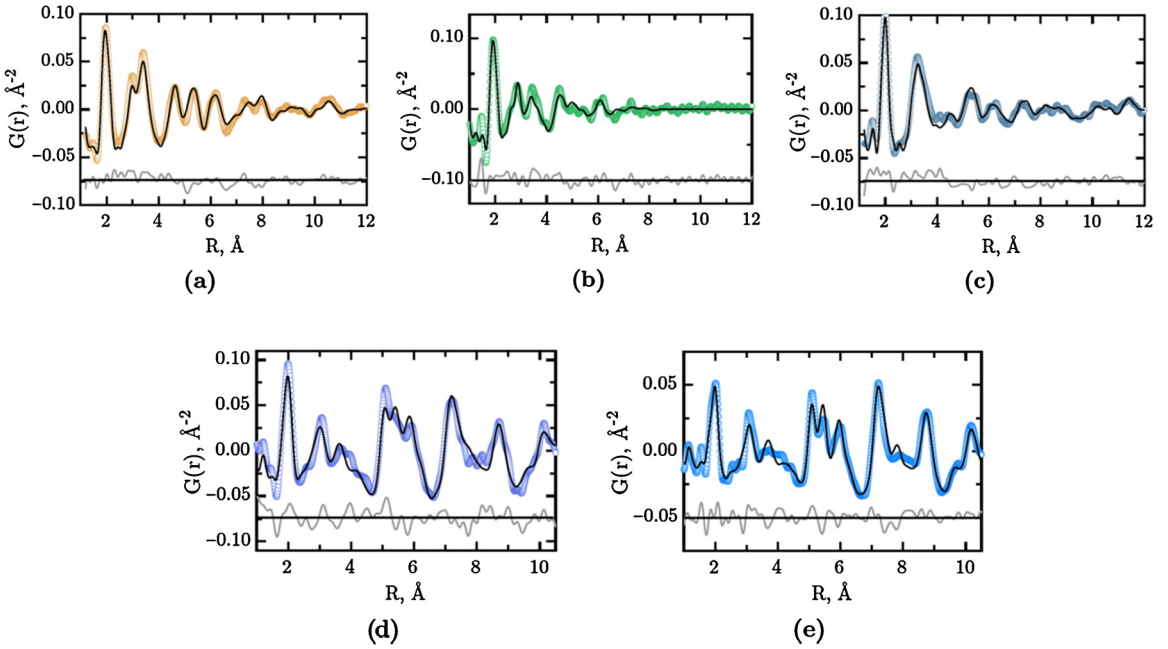

Fig. 11. Refinement of the PDF obtained on laboratory-synthesized 18th-century powder samples, (a): D2, $R_w = 21.8\%$; (b): LPA3, $R_{wp} = 31.8\%$; (c): LPA2, $R_{wp} = 25.7\%$; (d): D1, $R_{wp} = 29.6$; (e): LPA1, $R_{wp} = 24.8\%$. Experimental, calculated PDFs and fit residuals are shown as open colored circles and black and grey solid lines, respectively [12].

the isotypic aluminum hydrate phase could be present, namely tohdite, $Al_{10}O_{14}(OH)_2$, with $P6_3mc$ space group, $a = 5.58$ Å, $c = 8.86$ Å [23]. Finally, the PDFs of samples D1 and LPA1 were refined as single-phase PB, with the same vacancy-ordering model as described above for commercial soluble PB. For samples D2 and LPA3, a single tohdite phase was used, with possibility of Fe substitution on the Al site and complete absence of PB. The LPA2 sample was treated as a mixture of PB and ferrihydrite, yielding refined mass proportions of 10% and 90%, respectively [16]. The obtained fits are shown in Fig. 11.

As a conclusion of this study combined with several other characterization techniques, the original pale blue color prepared using 18th-century recipes is attributed to the presence of tohdite aluminum hydrate that can be eliminated by dissolution in an acid. The samples that exhibit the highest color evolution on ageing all contain a large amount of ferrihydrite that precipitated during the synthesis. Those that contain only Prussian blue and no alumina hydrate or iron oxide have a similar fading behavior as the commercial ones. It seems that ferrihydrite, as an undesirable hydrous iron oxide, causes the paint layers to turn green because upon ageing the Prussian blue phase fades and the orange tint of the ferrihydrite becomes more apparent. In this study, the contribution of PDF analysis was instrumental for the detailed study of the local structure of PB pigments, as well as the elucidation of the fading mechanism through the unambiguous identification of the ferrihydrite and tohdite phases.

4.2. PDF study of archaeological carbon blacks

Carbon black materials have been frequently used from prehistory as pigments for drawings and paintings and also as dyes, inks, and cosmetics. They could be easily obtained either from soot or lampblack, or by burning various types of organic matter (woods, bones, etc.). According to why they were used, they may have been mixed with other mineral phases or organic binders. The presence of foreign phases may also be due to pollution from the container, ageing of the preparation, etc. It is therefore particularly interesting to investigate such materials in terms of chemical composition, phase identification, and proportion and microstructure, aiming to elucidate their fabrication recipes and usage, origin of ingredients or evolution over time. However, this is not an easy task for the materials scientist, since the samples, besides being rare and precious, may contain complex organic/inorganic phases in very different proportions and microstructure, from amorphous phases to highly crystalline quartz grains. Moreover, the carbonaceous phases themselves are often ill ordered and their crystal structures are not well defined.

In a recent study [24], the association of Rietveld and PDF analysis with DSCT was used to provide detailed quantitative information not otherwise obtainable on archaeological carbon black samples from the Roman period. Five archaeological black powders were sampled from bronze and glass vessels found in houses in Pompeii, the shape of the containers suggesting their use as cosmetics or as inks. Modern black pigments to be used as references were either purchased from suppliers (bone, ivory, peach, and lamp black, graphite) or fabricated (charred wood). All were first characterized using optical microscopy, SEM and EDX analysis.

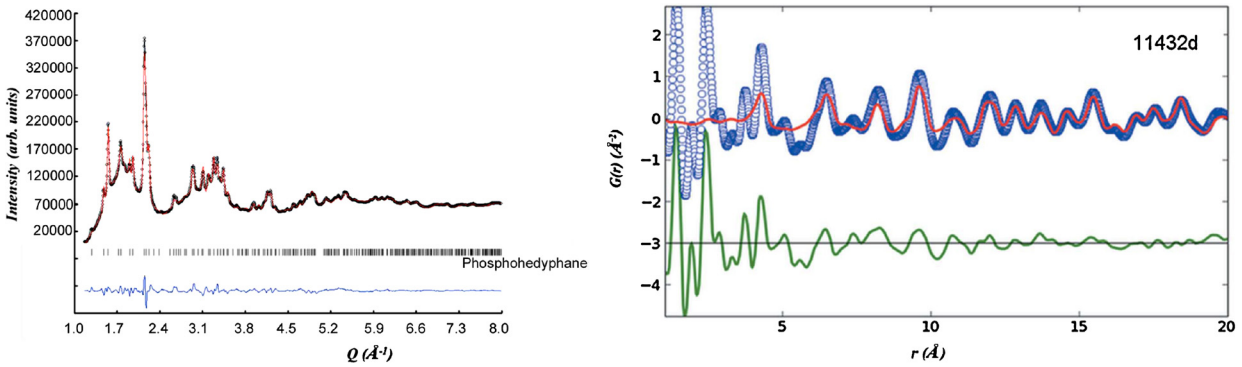

Fig. 12. Rietveld refinement (left) and extraction of the PDF of the amorphous fraction (right) for a Roman-period black pigment sample. The PDF of the amorphous fraction is obtained by the difference (green line) between the observed PDF (blue open circles) and the PDF of the crystalline fraction (red line) scaled to the experimental PDF in the 12–20 Å range.

Total scattering data were collected at the BM02-ESRF beamline with a 25-keV energy, using a CCD camera located at 120 mm from the sample. To reach a large enough Q_{max} of 20 $Å^{-1}$ for PDF analysis, images were recorded every 3° up to $2\vartheta = 100°$. The images were integrated and summed to yield 1D diffraction patterns that were then converted to PDFs using the PDFGetX2 software [17]. For the DSCT data collection, tomographic data sets were obtained by completing series of line scans covering ∼1 mm with an angular range from 0 to 180°, a 30-µm translation step size and a 12° rotation step size. The translation step was smaller than the beam size so as to obtain medium-resolution reconstructed images by direct analysis (voxel size: 30 × 30 × 100 µm), as shown by Alvarez-Murga et al. [25]. A reverse analysis was then carried out to extract a posteriori the diffraction signal from a selected area of the reconstructed image.

Due to the complexity of the samples containing a large diversity of crystalline as well as amorphous phases, the strategy employed was to first use XRPD and DSCT in addition to the SEM-EDX elemental analysis to locate, identify and quantify the different crystalline phases in each sample. Rietveld refinements were conducted to confirm the phase identification and to obtain the mass proportions in the case of crystalline phase mixtures. The PDF data were then used to identify the amorphous phases. For this purpose, the calculated PDF of the previously quantified crystalline phases with their relative proportions was scaled to the experimental PDF in a long-distance domain (between 12 and 20 Å) in which amorphous phases are estimated not to contribute. The short-distance range of the PDF corresponding to the contribution of the amorphous fraction was obtained by subtracting the scaled crystalline contribution from the experimental PDF (Fig. 12).

An example of this analysis is given for a particular sample (labeled 11432d) collected from a glassy *unguentarium* that was found to contain the quite rare mineral compound phosphohedyphane ($Ca_2Pb_3(PO_4)_3Cl$) as the only crystalline phase.

It is worth noting that this procedure was necessary since the DSCT and PDF data were recorded using a beam of moderately high energy that prevented one from obtaining PDF data at each point of the DSCT data collection. Moreover, the relatively large voxel size imposed by the beam size prevented one from extracting the patterns of the pure single phases by DSCT reverse analysis. Using a high energy (typically >60 keV), a size beam of a few microns, and a large 2D detector would allow one to collect PDF data in a single shot, which would greatly simplify the analysis process. On the other hand, this strategy can be applied using a laboratory instrument, using an Ag Kα microsource generator providing a beam size <200 µm, a 2D detector, and a translation/rotation system for DSCT data collection [26,27].

To identify the origin and nature of the amorphous phases, their PDFs were compared to the ones obtained for the modern references. For this purpose, fitting of the PDF using structural models of non-graphitic carbons [28,29] led to poor results: the interlayer spacing and the first C–C distances were in agreement with the presence of layer planes of graphite-like carbon, but the random distribution of oriented and disoriented layers as well as the non-flatness of individual graphene layers were difficult to take into account. A recent study on pyrocarbons [30] has shown that complex models using the image-guided atomistic reconstruction method based on HRTEM observation are required to interpret the PDF of such materials. Such type of modeling cannot be considered for even more complex and disordered archaeological samples. An alternative way to identify the amorphous phase is to quantify the similarity of the PDFs from archaeological and reference samples by computing the Pearson product momentum correlation R [31]:

$$R(X,Y) = \frac{1}{n-1}\sum_{i=1}^{n}\left(\frac{X_i - \overline{X}}{\sigma_X}\right)\left(\frac{Y_i - \overline{Y}}{\sigma_Y}\right)$$

where $\overline{X}$ and σ_X are the mean and standard deviation of a data set, respectively. $R = 1$ implies complete correlation, $R = 0$ no correlation, and $R = -1$ anticorrelation. The Pearson correlation technique is extremely powerful because it ignores absolute scaling, but is sensitive to relative scaling and slight shifts in peak position. It has recently proved its efficiency in amorphous pharmaceuticals fingerprinting [5,6].

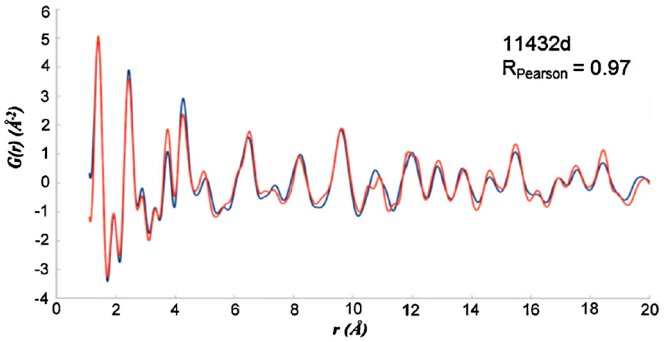

Fig. 13. Fit of the PDF of the same black pigment as in Fig. 11. Blue curve: experimental PDF; red curve: PDF calculated from the weighted sum of the experimental PDF of charred wood (amorphous fraction) and calculated PDF of phosphohedyphane (crystalline fraction). The proportion of the two fractions could be determined by optimizing the correlation between the two curves using the Pearson criterion over the full 1.00–20.00 Å range.

The Pearson correlation coefficients between the archaeological and the reference samples revealed a strong correlation with carbon black pigments derived from the combustion of plants: charred wood or peach black. This result reveals that Roman carbon blacks were not prepared from animal materials, as also suggested by the absence of apatite or hydroxylapatite demonstrated by XRPD, compounds that are always present in black pigments prepared from bone of ivory. For each archeological sample, using the experimental PDF from the best correlated reference sample and the PDF calculated from the crystalline phase content, it was also possible to reconstruct the full experimental PDF, thereby allowing the quantization of the amorphous phase in the sample (Fig. 13).

This example emphasizes the importance of the PDF analysis in the identification and quantification of amorphous phases in archeological samples, even containing mixed phases. It is also worth noting the role of DSCT in the identification of minor crystalline phases.

5. Conclusion

PDF analysis is not yet a widespread technique for the study of cultural heritage materials, probably due to the relatively recent availability of well-adapted and user-friendly equipment and software. However, we hope to have demonstrated its potential usefulness in this field, and there is no doubt that its use will increase with the development of new beamlines at synchrotron sources and laboratory instruments, and with the growing echo of the method in the scientific community.

Acknowledgements

The author wishes to warmly thank all colleagues who have participated in the studies described in this review, especially Pauline Martinetto, Louise Samain, Sophie Cersoy, Laurianne Religieux, Jean-Louis Hodeau, Nils Blanc, Nathalie Boudet, Olivier Leynaud, Erik Elkaïm, and Gavin Vaughan.

References

[1] A. Guinier, X-Ray Diffraction in Crystals, Imperfect Crystals, and Amorphous Bodies, Freeman, San Francisco, CA, USA, 1963.
[2] B.E. Warren, X-Ray Diffraction, Addison–Wesley Publishing Co., 1969.
[3] D.A. Keen, J. Appl. Crystallogr. 34 (2001) 172.
[4] T. Egami, S.J.L. Billinge, Underneath the Bragg Peaks: Structural Analysis of Complex Materials, 2nd edn., Pergamon, Oxford, UK, 2012.
[5] T. Dykhne, R. Taylor, A.J. Florence, S.J.L. Billinge, Pharm. Res. 28 (2011) 1041.
[6] T. Davis, M. Johnson, S.J.L. Billinge, Cryst. Growth Des. 13 (2013) 4239.
[7] C.L. Farrow, P. Juhas, J.W. Liu, D. Bryndin, E.S. Bozin, J. Bloch, T. Proffen, S.J.L. Billinge, J. Phys. Condens. Matter 19 (2007) 335219.
[8] J. Rodriguez-Carvajal, A. Bytchkov, Institut Laue-Langevin, Grenoble, France, 2016.
[9] G.F. Rust, J. Weigelt, IEEE Trans. Nucl. Sci. 45 (1) (1998) 75.
[10] P. Bleuet, E. Welcomme, E. Dooryhee, J. Susini, J.-L. Hodeau, P. Walter, Nat. Mater. 7 (6) (2008) 468.
[11] S.D.M. Jacques, M. di Michiel, S.A.J. Kimber, X. Yang, R.J. Cernik, A.M. Beale, S.J.L. Billinge, Nat. Commun. 4 (2013) 2536.
[12] L. Samain, PhD thesis, Université de Liège, Belgium, 2012.
[13] J.F. Keggin, F.D. Miles, Nature 137 (1936) 577.
[14] H.J. Buser, D. Scharzenbach, W. Petter, A. Lusi, Inorg. Chem. 16 (11) (1977) 2704.
[15] L. Samain, F. Grandjean, G.J. Long, P. Martinetto, P. Bordet, D. Strivay, J. Phys. Chem. C 117 (19) (2013) 9693.
[16] L. Samain, F. Grandjean, G.J. Long, P. Martinetto, P. Bordet, J. Sanyova, D. Strivay, J. Synchrotron Radiat. 20 (2013) 460.
[17] X. Qiu, J.W. Thompson, S.J.L. Billinge, J. Appl. Crystallogr. 37 (2004) 678.
[18] F. Herren, P. Fischer, A. Ludi, W. Halg, Inorg. Chem. 19 (1980) 956.
[19] R. Dossie, The Handmaid to the Arts, J. Nourse, London, 1758.
[20] M. Le Pileur d'Apligny, Traité des couleurs matérielles et de la manière de colorer relativement aux différents arts et métiers, Saugrain et Lamy, Paris, 1779.
[21] E. Murad, J.H. Johnston, in: G.J. Long (Ed.), Mössbauer Spectroscopy Applied to Inorganic Chemistry, vol. 2, Plenum Press, 1987, p. 507.
[22] F.M. Michel, L. Ehm, S.M. Antao, P.L. Lee, P.J. Chupas, G. Liu, D.R. Strongin, M.A. Schoonen, B.L. Phillips, J.B. Parise, Science 316 (2007) 1726.

[23] S.L. Hwang, P.Y. Shen, H.T. Chu, T.F. Yui, Int. Geol. Rev. 48 (2006) 754.
[24] S. Cersoy, P. Martinetto, P. Bordet, J-L. Hodeau, E. Van Elslande, P. Walter, J. Appl. Crystallogr. 49 (2016) 585.
[25] M. Alvarez-Murga, P. Bleuet, J.-L. Hodeau, J. Appl. Crystallogr. 45 (2012) 1109.
[26] P. Bordet, P. Martinetto, in: M. Descamps (Ed.), Disordered Pharmaceutical Materials, Wiley–VCH, Weinheim, Germany, 2016.
[27] S. Cersoy, O. Leynaud, M. Alvarez-Murga, P. Martinetto, P. Bordet, N. Boudet, E. Chalmin, G. Castets Hodeau, J. Appl. Crystallogr. 48 (2015) 159.
[28] R.E. Franklin, Acta Crystallogr. 3 (1950) 107.
[29] A. Burian, J.C. Dore, Acta Phys. Pol. A 98 (2000) 457.
[30] P. Weisbecker, J-M. Leyssale, H.E. Fischer, V. Honkimäki, M. Lalanne, G.L. Vignoles, Carbon 50 (4) (2012) 1563.
[31] K. Pearson, Proc. R. Soc. Lond. 58 (1895) 240.